Title	"In situ" hard mask materials: a new methodology for creation of vertical silicon nanopillar and nanowire arrays
Authors	Ghoshal, Tandra;Senthamaraikannan, Ramsankar;Shaw, Matthew T.;Holmes, Justin D.;Morris, Michael A.
Publication date	2012-12
Original Citation	Ghoshal, T., Senthamaraikannan, R., Shaw, M. T., Holmes, J. D. and Morris, M. A. (2012) '"In situ" hard mask materials: a new methodology for creation of vertical silicon nanopillar and nanowire arrays', Nanoscale, 4(24), pp. 7743-7750. doi: 10.1039/C2NR32693K
Type of publication	Article (peer-reviewed)
Link to publisher's version	http://pubs.rsc.org/en/Content/ArticleLanding/2012/NR/c2nr32693k - 10.1039/C2NR32693K
Rights	© Royal Society of Chemistry 2012
Download date	2024-09-26 16:13:05
Item downloaded from	https://hdl.handle.net/10468/6783

"Insitu" hard mask material: A new methodology for creation of vertical silicon nanopillar and nanowire arrays

Tandra Ghoshal,[1,2] Ramsankar Senthamaraikannan,[1,2] Matthew T. Shaw,[1,2,3] Justin D. Holmes,[1,2] and Michael A. Morris [1,2*]

----

[1]Materials research group, Department of Chemistry and Tyndall National Institute, University College Cork, Cork, Ireland

[2]Centre for Research on Adaptive Nanostructures and Nanodevices (CRANN), Trinity College Dublin, Dublin, Ireland

[3]Intel Ireland Ltd., Collinstown Industrial Estate, Co. Kildare, Ireland

[*] Corresponding Author: Prof. Michael A. Morris

E-mail: m.morris@ucc.ie

Tel: + 353 21 490 2180

Fax: ++353 21 427 4097

A novel, simple and insitu hard mask technology that can be used to develop high aspect ratio silicon nanopillars and nanowire features on a substrate surface is demonstrated. The technique combines a block copolymer inclusion method that generates nanodot arrays on substrate and an inductively coupled plasma (ICP) etch processing step to fabricate Si nanopillar and nanowire arrays. Iron oxide was found to be an excellent resistant mask over silicon under the selected etching conditions. Features of very high aspect ratio can be created by this method. The nanopillars have uniform diameter and smooth sidewalls throughout their entire length. The diameter (15-27 nm) and length of the nanopillars can be tuned easily. Different spectroscopic and microscopic techniques were used to examine the morphology and size, surface composition and crystallinity of the resultant patterns. The methodology developed may have important technological applications and provide an inexpensive manufacturing route to nanodimensioned topographical patterns. The high aspect ratio of the features may have importance in the area of photonics and the photoluminescence properties are found to be similar to those of surface-oxidized silicon nanocrystals and porous silicon.

Introduction

Silicon and its one-dimensional nanostructures has become essential for potential applications in integrated optoelectronic nanodevices.[1-3] Thus, the fabrication of vertically aligned iso-axial Si nanostructured arrays is becoming very important. However, accurate control over the axial crystallographic orientation of these nanostructures is necessary as it significantly influences their electronic structure (energy gap) as well as their physical properties (electronic transport).[4-5] This Strict control of crystallography is required for the realization of advanced device technologies including electronic field emission, chemical sensing, field effect transistors, solar cells as well as biosensing.[6-9] Of particular relevance is the possibility of visible photoluminescence (PL) from porous Si because of applications as light sources as well as potential for development of novel flash memory.[10-11] Of course, for many

applications, it is not only crystallographic control that is necessary but also the diameter, spacing and shape of the vertical nanostructures which need to be fabricated precisely over large areas with high throughput and low cost. Fabrication normally requires a UV-lithographic approach using a mask and etch process to fabricate the crystallographically aligned and dimension controlled silicon nanostructures. E-beam lithography is usually used to realise the smallest feature size structures but is of prohibitive cost and low throughput.[12] As an alternative approach, self-assembly might have importance. The microphase separation of block copolymer (BCP) thin films can provide uniform densely spaced nanometer-scale features over wafer scale areas and is simple and cost-effective. The BCP nanopatterns can be integrated into a lithographic method by selective removal of one block and then using the remaining polymer as an etch mask for pattern transfer into the substrate.[13-16] However, the technique is limited for optical device application because the features generated tend to have low aspect ratio since the films generally have thicknesses around that of the BCP domain spacing and this results in poor etch selectivity and shape control.[17] The quality of the etch and the features formed greatly reduce the quality factor of the device.[18] To overcome this barrier, a 'hard mask' photoresist material with extremely high selectivity could be used. Dielectric materials (SiO_2, Al_2O_3 and Si_3N_4 etc.), various metal oxides and metals have been used as a etch masks.[19-22] Dielectric materials have much higher selectivity than conventional photoresists but require multi-step pattern transfer processes from the pre-fabricated pattern.[19] Metals (Cr, Ni), with high selectivity, are usually patterned by a lift-off technique but this can result significant distortion of the patterns and metal etching can present challenges.[20, 23] It is also highly undesirable for the hard masks to be a permanent part of a device structure. Hence to enable BCP lithographic methods for realisation of high aspect ratio features there is a strong requirement to develop a methodology where a hard mask approach can be integrated into the BCP process and provide a facile, inexpensive patterning process.

In this paper we demonstrate a method to generate a patterned inorganic oxide hard mask material (iron oxide) via a simple and cost-effective diblock copolymer inclusion technique. The hard mask enables extremely high pattern transfer fidelity into silicon with a capability to produce structures orders of magnitude thicker than the original mask thickness. Using inductively coupled plasma (ICP) dry etch techniques, the fabrication of the densely packed, size uniform, high aspect ratio silicon nanopillar and nanowire arrays with good sidewall profiles can be shown. ICP etch methods are an advanced and sophisticated processes to provide highly anisotropic profiles with excellent control over selectivity to mask materials using low pressure plasmas which generates high density ion fluxes. Further, by independently controlling both the plasma density and the momentum imparted to the ions, significant improvements in control of the structures can be attained. We also show that the hard mask used can be easily removed with any significant pattern damage.

Experimental Section

Single crystal B doped P type silicon (100) wafers (Thickness 650 μm, resistivity 6-14 ohm-cm) with a native oxide layer were used as a substrate. These were cleaned by ultrasonication in acetone and toluene for 30 min each and dried under a nitrogen stream. The detail of the preparation of iron oxide nanodot array was described elsewhere.[24-25] Polystyrene-b-poly(ethylene oxide) (PS-b-PEO) diblock copolymer was purchased from Polymer Source Inc. and used without further purification (number-average molecular weight, M_n, PS = 42 kg mol^{-1}, M_n, PEO = 11.5 kg mol^{-1}, M_w/M_n = 1.07, M_w: weight-average molecular weight). PS-b-PEO was dissolved in toluene to yield 0.9 wt% polymer solution at room temperature. The PS-b-PEO thin film was formed by spin coating the polymer solution (3000 rpm for 30 s). The film was exposed to toluene/water (50:50, v/v) mixed vapour placed at the bottom of a closed vessel kept at 50^{0}C for 1h under static vacuum. The film was immersed in ethanol at 40 ^{0}C for 15 h to obtain the activated film. Different concentration iron (III) nitrate

nonahydrate (Fe(NO$_3$)$_3$,9H$_2$O) in ethanolic solutions were spin-coated onto the activated film. UV/Ozone treatment was used to oxidize the precursor and remove polymer. The nanodots were further annealed at 800^{0}C for 1h. These iron oxide nanodot arrays were used as a hard mask for pattern transfer onto the substrate. Pattern transfer was accomplished using an STS, Advanced Oxide Etch (AOE) ICP etcher. The system has two different RF generators, one, to generate and control the plasma density by direct connection to the antenna coil, while the other one was used to adjust and control the energy of ions by connecting it to the substrate holder. A double etching process was used to, firstly, etch the native silica layer and, secondly, the silicon substrate. During etching, the sample is thermally bonded to a cooled chuck (10^{0}C) with a pressure 9.5 Torr. For the oxide layer etch, the process parameters were optimised to a C$_4$F$_8$/H$_2$ gas mixture (21 sccm/30 sccm) using an ICP coil power of 800 W and a Reactive Ion Etching (RIE) power of 80 W. The silica etch time was kept constant (10 sec) for all the samples. For Si pillar fabrication, the process used a controlled gas mixture of C$_4$F$_8$/SF$_6$ at flow rates of 90 sccm/30 sccm respectively and the ICP and RIE power were set to 600 W and 15 W respectively at a chamber pressure of 15 mTorr. The height of the Si pillars was varied by simply varying the Si etch time. For the removal of iron oxide nanodots, the substrate was immersed into 10 wt% aqueous solution of oxalic acid dihydrate (C$_2$H$_2$O$_4$, 2H$_2$O) for 2 hours at room temperature, washed with water several times and dried.

Surface morphologies were imaged by scanning electron microscopy (SEM, FEI Company, FEG Quanta 6700 and Zeiss Ultra Plus). Samples were prepared for TEM cross sectional imaging with Zeiss Auriga - Focused Ion Beam (FIB) dual beam system containing a high resolution field-emission SEM and Ga+ cobra ion columns with 2.5 nm resolution and were further imaged by transmission electron microscopy (TEM, FEI Titan). X-Ray photoelectron spectroscopy (XPS) experiments were conducted on a Thermo K-alpha machine with Al K$_\alpha$ X-ray source operating at 72 W. FTIR spectra were recorded on infrared spectrometer (IR

660, Varian). The photoluminescence measurements were carried out at room temperature with a fluorescence spectrophotometer (Perkin-Elmer LS 50 B). Raman spectra were recorded using a SPEX 1403 monochromator equipped with a dc detection device. The 488 nm laser line of an Ar ion laser was used for excitation with an output power of 20 mW.

Results and Discussion

The methodology of preparing ordered arrays of iron oxide nanodots was based on formation of a microphase separated PS-b-PEO thin films by solvent annealing.[26] This provides a nanopattern consisting of hexagonally arranged, vertically oriented (to the surface plane) of PEO cylinders in PS matrix. The marked chemical difference between PS and PEO allows the selective inclusion of metal ions into the PEO block and avoids any component removal. Prior to the inclusion of the inorganic component, the PEO blocks were 'activated' by ethanol which accelerates the inclusion of metal cations or colloidal entities into the cylinders probably via either intra- or intermolecular coordination through electron donation from the PEO block oxygen atoms. UV/ozone treatment was used to convert the polymer-inorganic component combination into a rigid oxide pattern and is effective because of its' ability in converting non-volatile inorganic compounds into oxides whilst removing organic components. The as prepared iron oxide (Fe_3O_4) nanodots have uniform size and shape and their placement mimics the original self-assembled block copolymer pattern. The nanodots have good thermal stability and strong adherence to the substrate surface but the annealing at 800 ^{0}C causes the transformation of the phase to Fe_2O_3.

Scheme 1 illustrates the process flow diagram of the fabrication of ordered aligned Si nanopillars by pattern transfer into Si substrate using iron oxide nanodots as a hard mask. Scheme 1A shows the formation of a hexagonal array of iron oxide nanodots on the substrate prepared by block copolymer inclusion technique as described above. A rapid silica etch process is followed to remove the exposed native silica layer on top of the substrate whereas

the oxide layer underneath iron oxide nanodots (mask) remained unaffected (Scheme 1B). The pattern transfer process is pursued by the Si etch process during which the substrate area directly below the mask is protected from the etch gases and only the exposed silicon is removed. This process results in the formation of the Si nanopillars with a layer of native oxide and iron oxide at their uppermost surface as illustrated in Scheme 1C. The Si nanopillars with same structural arrangement and lateral dimension are obtained after removal of iron oxide nanodots (Scheme 1D).

Fig. 1a shows dense (4.2×10^{10} cm^{-2}) hexagonally ordered iron oxide (Fe_2O_3) nanodots on the substrate prepared by the BCP inclusion technique. The nanodots are well adhered to the substrate after annealing at 800^0C for 1h, with a diameter 21 nm, height 7 nm and the centre to centre nanodot spacing 42 nm. Pattern transfer via silica and silicon etches created Si nanopillar arrays with Fe_2O_3 nanodots at top of the pillars. The top-down SEM image (Fig. 1b) demonstrates a densely packed, uniform, ordered arrangement over large areas after the pattern transfer. The significant contrast enhancement (compared to Fig. 1a) suggests pattern transfer has occurred. The high resolution SEM image in the inset of Figure 1b also reveals the hexagonal ordered pillars have an average diameter of 21 nm at a spacing of 42 nm. This implies that the etching does not damage the original pattern to any extent. A mild oxalic acid aqueous solution was used to remove the undesired Fe_2O_3 mask from the top of Si nanopillar arrays. Fig. 1c shows the structures are unaltered by the oxide removal and show only silicon structures with a native silica layer at their upper surface. The average height of the Si nanopillars is around 500 nm (measured from the cross-sectional SEM image shown in Fig. 1d) for a 10 minute Si etch time. The higher magnification image in Fig. 1d (bottom) shows the pillars of uniform diameter along their length and no shadowing effect of mask is observed. Further, smooth sidewalls are observed.

Fig. 2a shows FTIR absorption spectra of the etched sample before (I) and after (II) iron oxide removal to reveal the composition of the Si nanopillars on Si substrate. Two major features centred at 678 cm^{-1} and 1070 cm^{-1} are detected for both the samples. The band centred at 678 cm^{-1} can be assigned to neutral charged oxygen vacancies possibly nonbridging oxygen hole centers (NBOHCs) or similar compounds in β-cristobalite, a silica polymorph.[27] It has also been reported that the peaks between 660–690 cm^{-1} are an indicative of high density Si-Si bonds.[28] Since the peak is present for both the samples and silica is a minor component in these samples, the second assignment is much more likely and suggests that the major component is silicon for both the samples and that the pillars are largely silicon in nature as will be confirmed below. The feature at 1070 cm^{-1} is associated with stretching vibration modes of the Si-O-Si bonds in SiO$_2$.[29] For clarity, the insets shows corresponding magnified spectra in the range between 1000-1300 cm^{-1}. As these peaks do not undergo any important changes, it can be argued that no restructuration occurs during iron oxide removal process. An additional strong peak at 540 cm^{-1} is observed for the etched sample (Fig. 2a(I)) and corresponds to the most intense peak for hematite.[30] This peak disappeared after oxalic acid treatment (Fig. 2a(II)) and so confirms removal of the iron oxide nanodot component. The spectra also showed bands centred at 1170 cm^{-1} and 1235 cm^{-1} are assigned to C-F stretching vibrations.[31] The band at 1235 cm^{-1} corresponds to a C-F stretching vibration where covalent bonding predominates.[32] These peaks are typical of substrates etched with fluorine containing gases.[33]

In order to quantify the surface composition, XPS analyses were performed on the etched samples before and after iron oxide removal process. Fig. 2b shows typical XPS survey spectrum of the sample after a 3 min Si etch and confirms the presence of Si, C, O, F and Fe. The Si, O and Fe features originate from the Si nanopillars, the native oxide layer and iron oxide nanodots at the top of the pillars respectively. However, the intensity of C1s feature is

significantly greater than might be expected from adventitious contamination during sample preparation etc. It is likely that the F1s peak is formed during the etch process (as there was no sign of fluorine before etching). To investigate further, additional high resolution C1s, F1s and Fe2p spectra were recorded. Fe 2p core level spectrum (inset of Fig. 2b) consists of two sharp peaks associated with Fe $2p_{3/2}$ and Fe $2p_{1/2}$ at 711.3 and 725.1 eV accompanied by high binding energy satellite structures (+8 eV shift). The absence of a feature at 714.5 eV implies that metal fluoride (FeF_3) is not produced during the etch process.[34] These data are consistent with the existence of Fe^{+3} (Fe_2O_3) ions only.[35] The C1s spectrum shown in Fig. 2c exhibits two major components at 285 eV and 289.2 eV. The peak at 285 eV is assigned to adventitious carbon and the other peak is attributed to the carbon atoms covalently bonded to the fluorine atoms (C-F bond).[36] The F1s XPS spectrum (inset of Fig. 2c) exhibits a sharp peak at 689.3 eV corresponds to fluorinated carbon atoms (C-F).[36] The absence of a metal fluoride peak (around 685 eV) again confirms only the Fe_2O_3 phase is present in the sample.[34] These results suggest the generation of perfluorinated C-F (CF_2 or CF_3) during the etch process. Fig. 2d shows the survey spectrum of the etched sample after iron oxide removal clearly implies effective removal of iron oxide. All other peaks remain unaffected and suggest that the oxalic acid solution has little or no effect on the structure. The intensity of the Si features increases as the iron is removed as might be expected. The high resolution Si 2p spectrum (inset of Fig. 2d) provides information about nature of the Si and its compounds. The spectrum consists of one strong peak at 99.3 eV corresponding to zero-valent Si and another weak peak at 103.4 eV assigned to the silicon oxide phase close to silica. Hence, the XPS results confirm the presence of silicon nanopillars on the substrate with a native oxide layer at top.

The diameters and heights of the resultant patterns can be varied by changing the diameter of the oxide mask and the Si etch time respectively without altering other processing

conditions. At the longer etch times, well defined nanowire arrays can be formed. Figs. 3a, b, c, d and e shows the cross-sectional SEM images of the hexagonal patterned uniform Si nanopillars (or nanowires) with vertical smooth sidewalls of average heights about 50 nm, 100 nm, 150 nm, 400 nm and 500 nm for 1 min, 2 min, 3 min, 8 min and 10 min Si etch periods respectively. All the images demonstrate good coverage of the nanopillar/nanowire arrays over a large area. The diameters of the nanopillars are almost equal throughout its entire length, no narrowing or broadening effects are observed. The images reveal quite narrow distribution of the aspect ratio of the pillars. The higher magnification images shown in the inset of Fig. 3c and d exhibits vertical rows of silicon pillars of height 150 nm and 400 nm for 3 min and 8 min Si etch times. The variation of average nanopillar height with the Si etch time is shown in the inset of Fig. 3e. The nanopillars height increases linearly with etch time at a constant rate 50 nm min^{-1}. Different iron oxide nanodot diameters (by changing the concentrations of the iron precursor[24]) are employed produce Si nanopillars with different diameters. A large area SEM image (Fig. 3f) shows the ordered arrangement of the pillars of average diameter 27 nm and height 150 nm. Hexagonal featured aligned Si pillars of average diameter 15 nm can be accomplished with 3 min etch time (inset of Fig. 3f). From the SEM images, a very narrow distribution of the iron oxide nanodot diameters was observed and this, in turn, produces nanopillars of uniform diameter over the entire sample area. The diameters of the nanodots can only be varied over a narrow size range of 15-27 nm for the particular PS-b-PEO BCP used here, but it should be noted that the diameters as well as the spacing between the nanodots can be altered by use of BCPs of different molecular weight. It is noted that different concentrations of the iron precursor solution altered the nanodot diameter as well as the thickness of the resultant nanodots (which is clearly an important parameter in the pattern transfer process). As the precursor solution prepared typically consists of a large volume fraction of ethanol, the free volume of the PEO activated cylinders is predominantly

filled by ethanol, thus, the quantity of the inorganic component within the PEO cylinders depends on the concentration of the precursor used. In this way, the diameter and thickness of the nanodots are directly proportional to the precursor concentration to a certain extent. Thus, different aspects ratio nanopillars can be realized either by changing the diameter of the mask or by varying the etch time. No surface roughening or pattern damage is seen with decreasing the diameter or increasing the height of the pillars.

Fig. 4a and b shows the cross sectional TEM images of the array of etched (60 sec) nanopillars fabricated on (100) Si substrates, before and after iron oxide removal respectively. The images reveals ordered arrays of Si nanopillars of about 50 nm long with the expected 42 nm centre-to-centre spacing between them. Fig. 4a clearly shows the iron oxide nanodots with distinct contrast difference at the top of the pillars. These features are completely removed after the acid removal process (Fig. 4b). The higher magnification TEM image shown in the inset of Fig. 4a reveals the layered arrangement of silicon, silicon oxide, iron oxide at the top of the nanopillars. All the pillars were found to maintain a rectangular profile with smooth sidewalls and there is almost no diameter variation along the length. Note that the nanopillars are not damaged during the oxide removal process and their original profiles and arrangement are unchanged (Fig. 4b). Direct high resolution TEM imaging of the pillars following FIB thinning was not possible because of silica deposition during the FIB treatment. In order to reveal the crystalline structure of the Si nanopillars after the oxide removal process, Pt was directly deposited onto the nanopillars and samples FIB thinned. Fig. 4c shows identical ordered arrays (front and back rows) of Si nanopillars after iron oxide removal. The EDAX spectrum obtained along the length of the nanopillars reveals the presence of Si, Cu and Pt (inset of Fig. 4c). The absence of Fe again proves the effective removal of the iron oxide. In the HRTEM image, ordered atomic planes i.e single crystalline structure can be observed on two of the nanopillars shown in Fig. 4d (left). The higher

resolution image of the marked area shows the lattice fringes with a spacing 3.12 Å across the pillars agrees reasonably well with cubic fcc structure of Si (111) lattices planes.[37] The nanopillars were axially oriented at angle 54^0 with the (111) lattice planes and is consistent with a (100) growth direction i.e. identical to the orientation of the initial Si wafer. Thus, highly dense uniform 1D silicon nanopillar arrays with controlled crystallographic orientation could be created through selective etching of the silicon wafers of chosen orientations. TEM also reveals a very thin amorphous layer at the surfaces of the nanopillars and this might be either a native oxide or residual C-F polymer formed by etching. Fig. 4d (right) shows the continuous clear lattice fringes across the junction between Si wafer and the nanopillar indicates the absence of defects or stacking faults formed during etching.

The crystalline property of the Si nanopillars on Si substrate was further examined by Raman spectroscopy. The Raman spectrum obtained is nearly Lorentzian in shape and an intense peak is observed at 520 cm^{-1} and can be readily assigned to the first order transverse optical phonon mode of crystalline silicon (inset of Fig. 4c). This peak observed is in the centre of the Brillouin zone which is due to the conservation of quasi-momentum in crystals. The absence of other peak in Raman spectra confirms that the nanopillars retain the crystallinity of bulk silicon wafer.

Photoluminescence (PL) measurements were performed on the ordered arrays of Si nanopillars on the Si substrate aged for 10 days in ambient air. For the measurement, all the samples were immersed in oxalic acid solution (to remove the hard mask iron oxide nanodots), dried and placed at ambient air. The PL spectra of all the samples are almost similar, no apparent band shift or intensity difference was observed. Fig. 5 shows the PL spectrum of the Si nanopillars created after 3 minutes Si etch on Si wafer at room temperature. The PL band is intense with a Gaussian-like characteristics centred at 666 nm (~1.86 eV) under a 325 nm excitation wavelength. The same PL spectral region has been

reported in literature for different Si/SiO$_2$ based structures.[38-41] This band position is typical for non-bridging oxygen hole centres (NBOHC) in bulk silica.[42] Note that the NBOHC model of light emitters has also been suggested to explain visible PL from porous silicon[43] and Qin et al.[44-45] explained the visible emission from native oxide on Si wafers which originates from luminescent centres exist in the silica skins of nano-Si particles. As the pillars fabricated here are exposed to ambient air, there is always a native oxide layer exists on top as well as sidewalls of the Si nanopillars. It is, therefore, suggested that the PL band from the Si nanopillar arrays is associated with the native oxide exist at the top/sidewall of the pillars. Further, it is suggested that the luminescent centres originate from the oxygen deficient defects in the Si-SiO$_2$ interface region. It is noted that the PL intensity will be dependent on the aging time (i.e. oxide thickness) and also with the increase of height of the Si nanopillars.

The methodology used here was centered around a pattern transfer technique using an 'insitu' iron oxide hard mask process combined with a carefully tuned plasma etc. It is worthwhile discussing the etch chemistry in some detail. In order to provide the structural control of features needed, ICP power and DC bias were set to low-to-moderate levels to avoid heating of the samples, while gas flow rates were chosen to provide short gas residence times and hence an ample supply of etch species. The thin layer of silicon dioxide was etched using a combination of C$_4$F$_8$/H$_2$ gases. C$_4$F$_8$ exhibited highest silica etch rate among a series of fluorocarbon gases used but pure C$_4$F$_8$ gas flows showed poor etch selectivity presumably because of high concentrations of F atoms/radicals formed in the plasma.[46] The addition of hydrogen reduces the silica etch rate due to reduction of reactive species by simple dilution and also by the formation of HF. This also helps in the formation of CF$_x$ (x $\leq$ 2) radicals which increases the etch selectivity conformity through the formation of carbon-fluoro polymers at the sidewall.[33] Fluorine gas chemistry was used to etch the silicon substrate. To avoid sidewall corrugation or scalloping, a sequential etch/deposition process was used. The

chopping Bosch Si etch technique[47] is utilized which can be realized by sulphur hexafluoride, SF_6, as the etching gas and octafluorocyclobutane, C_4F_8, as the passivation gas. During etching step, SF_6 was injected into the chamber from which atomic fluorine can be generated by different collision processes in the plasma. These ions are driven down to the substrate by the electric field derived from the potential between the plasma and the substrate. Atomic fluorine is an aggressive radical that reacts with unmasked silicon through the reaction:

$$Si + 4F \rightarrow SiF_4$$
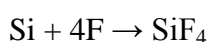
Where SiF_4, tetrafluorosilane is a volatile etch product and was removed by pumping. After few seconds of etch step, SF_6 is terminated instantly and C_4F_8 gas is injected into the chamber to begin the passivation phase. During this phase, CF_2 is formed from C_4F_8, which adsorbs on the etched surfaces and forms a teflon-like polymer passivation layer.

$$n\, CF_2 + * \rightarrow (CF_2)_n$$
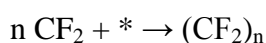
The process is then again switched to the etch step where CF_2 molecules are removed by combination of physical ion sputtering and chemical reactions. Due to directional ion bombardment of the substrate, polymer removal rate is greater for the horizontal surfaces, thus the sidewalls remains protected during the etch phase. A well balanced gas flow rates, etch times, and deposition steps were key to attaining high aspect ratio patterns with vertical sidewalls. Also, as the substrate temperature is 10^0C, the polymer passivation layer was far from both the melting and freezing regimes, and this was also necessary for the production of smooth and vertical sidewalls. Though the process is terminated with an etch phase and a well balanced phases are timed, but still there is issues of incomplete polymer removal as revealed by XPS studies. A very thin amorphous polymer layer might exist on the sidewalls of the pillars as observed in HRTEM (Fig. 4d) otherwise they will be correlated with the broadening of the base. However, the Teflon-like polymer can be useful as an anti-stiction film.[48]

The selection of mask material is an important factor to control over primarily on aspect ratio of the features, sidewall profile and etch roughness. A higher selectivity of the mask over silica and silicon is required to achieve the desired features because the mask interacts with the etching process parameters. No narrowing of the base of the pillars was observed indicates robust nature of the mask. It is believed that there is no measurable degradation of iron oxide nanodots during the etch processes as their dimensions remains unchanged and the unaltered chemical composition of the oxide phase can be observed. The oxygen gas was strictly excluded from the chamber as it erodes the mask and retards the Si etch rate. As reported by Nakayama et al. that a thin iron oxide layer can perform as an excellent resistant mask to iron fluoride formation in the absence of oxygen.[49] Similarly, the erosion of Ni mask was seen to decrease with the oxygen content as it forms a thin oxide layer on the surface.[23] The methodology described here offers the advantage of high mask resolution on small feature sizes (~ 15 nm) without mask-induced roughness or undesired sloping of the sidewalls. To date, there are some reports on the use of metal and oxide masks (Ga, SiO_2, alumina etc.) with good selectivity but either they are grown or deposited as uniform layers followed by pattern transfer (from another material or resist) to that mask and this increases the number of processing steps or suffers from challenges with mask removal without pattern damage.[19, 50-51] Here, we have demonstrated iron oxide as an easy removable highly selective mask material over silicon. The relatively simple mask fabrication procedure with the standard existing etch recipes could significantly improve the manufacturing yield and reduce fabrication costs.

Conclusions

In summary, we have demonstrated the iron oxide nanodots prepared by a simple and cost effective block copolymer inclusion technique are an excellent resistant mask for silicon under the etch conditions that were developed. Large area ordered periodic rectangular cross

section Si nanopillar or nanowire arrays is fabricated with a smooth vertical sidewall profiles. The diameter and length of the nanopillars was precisely controlled by changing the diameter of the nanodots and increasing the etching time respectively without altering their shape. The effect of the etching parameters on the mask and the substrate is demonstrated in terms of the mask stability and interactions between them. The hard mask could be easily removed without significant pattern damage. The nanopillars observed were crystalline with desirable uni-axial crystallographic orientation. NBOHC was suggested as the source of light emission from the Si nanopillar arrays similar to that seen for porous silicon. The large area controlled periodic Si nanopillar arrays with desirable crystallographic orientation that are fabricated here demonstrate that BCP lithography can be an important component in the manufacturing of future nanoscale devices that employ silicon.

Acknowledgements

References

1 D. D. D. Ma, C. S. Lee, F. C. K. Au, S. Y. Tong and S. T. Lee, *Science* 2003, **299**, 1874.

2 Y. Cui and C. M. Lieber, *Science* 2001, **291**, 851.

3 X. Y. Zhao, C. M. Wei, L. Yang and M. Y. Chou, *Phys. Rev. Lett.* 2004, **92,** 236805-1.

4 C. Delerue, G. Allan and M. Lannoo, *Physical Review B* 1993, **48**, 11024.

5 H. Yorikawa, H. Uchida and S. Muramatsu, *J. Appl. Phys.* 1996, **79**, 3619.

6 M. R. Rakhshandehroo and S. W. Pang, *J. Vac. Sci. Technol. B* 1996, **14**, 612.

7 A. A. Talin, L. L. Hunter, F. Leonard and B. Rokad, *Appl. Phys. Lett.* 2006, **89**, 153102.

8 J. Zhu, C. M. Hsu, Z. F. Yu, S. H. Fan and Y. Cui, *Nano Lett.* 2010, **10**, 1979.

9 A. K. Wanekaya, W. Chen, N. V. Myung and A. Mulchandani, *Electroanalysis* 2006, **18**, 533.

10 M. V. Wolkin, J. Jorne, P. M. Fauchet, G. Allan and C. Delerue, *Phys. Rev. Lett.* 1999, **82**, 197.

11 S. Tiwari, F. Rana, H. Hanafi, A. Hartstein, E. F. Crabbe and K. Chan, *Appl. Phys. Lett.* 1996, **68**, 1377.

12 G. M. Wallraff and W. D. Hinsberg, *Chem. Rev.* 1999, **99**, 1801.

13 C. C. Liu, P. F. Nealey, Y. H. Ting and A. E. Wendt, *J. Vac. Sci. Technol. B* 2007, **25**, 1963.

14 M. Park, C. Harrison, P. M. Chaikin, R. A. Register and D. H. Adamson, *Science* 1997, **276**, 1401.

15 R. A. Farrell, T. G. Fitzgerald, D. Borah, J. D. Holmes and M. A. Morris, *Int. J. Mol. Sci.* 2009, **10**, 3671.

16 R. A. Farrell, N. Petkov, M. T. Shaw, V. Djara, J. D. Holmes and M. A. Morris, *Macromolecules* 2010, **43**, 8651.

17 D. Borah, M. T. Shaw, S. Rasappa, R. A. Farrell, C. O'Mahony, C. M. Faulkner, M. Bosea, P. Gleeson, J. D. Holmes and M. A. Morris, *J. Phys. D-Appl. Phys.* 2011, **44**, 174012.

18 M. Barth, J. Kouba, J. Stingl, B. Lochel and O. Bensona, *Opt. Express* 2007, **15**, 17231.

19 Q. L. Fang, X. D. Li, A. P. Tuan, J. Perumal and D. P. Kim, *J. Mater. Chem.* 2011, **21**, 4657.

20 K. M. Lim, S. Gupta, C. Ropp and E. Waks, *Microelectron. Eng.* 2011, **88**, 994.

21 I. W. Rangelow, *Vacuum* 2001, **62**, 279.

22 S. Krishnamoorthy, K. K. Manipaddy and F. L. Yap, *Adv. Funct. Mater.* 2011, **21**, 1102.

23 H. Y. Hsieh, S. H. Huang, K. F. Liao, S. K. Su, C. H. Lai and L. J. Chen, *Nanotechnology* 2007, **18**, 505305.

24 T. Ghoshal, T. Maity, J. F. Godsell, S. Roy and M. A. Morris, *Adv. Mater.* 2012, **24**, 2390.

25 T. Ghoshal, M. T. Shaw, C. T. Bolger, J. D. Holmes and M. A. Morris, *J. Mater. Chem.* 2012, **22**, 12083.

26 P. Mokarian-Tabari, T. W. Collins, J. D. Holmes and M. A. Morris, *ACS Nano* 2011, **5**, 4617.

27 T. Morioka, S. Kimura, N. Tsuda, C. Kaito, Y. Saito and C. Koike, *Mon. Not. Roy. Astron. Soc.* 1998, **299**, 78.

28 T. Inokuma, Y. Kurata and S. Hasegawa, *J. Lumines.* 1998, **80**, 247.

29 P. G. Pai, S. S. Chao, Y. Takagi and G. Lucovsky, *J. Vac. Sci. Technol. A-Vac. Surf. Films* 1986, **4**, 689.

30 H. Namduri and S. Nasrazadani, *Corrosion Sci.* 2008, **50**, 2493.

31 W. Zhang, M. Dubois, K. Guerin, P. Bonnet, H. Kharbache, F. Masin, A. P. Kharitonov and A. Hamwi, *Phys. Chem. Chem. Phys.* 2010, **12**, 1388.

32 Z. Gu, H. Peng, R. H. Hauge, R. E. Smalley and J. L. Margrave, *Nano Lett.* 2002, **2**, 1009.

33 T. Standaert, M. Schaepkens, N. R. Rueger, P. G. M. Sebel, G. S. Oehrlein and J. M. Cook, *J. Vac. Sci. Technol. A-Vac. Surf. Films* 1998, **16**, 239.

34 J. Q. Yang, Y. Liu, Z. Y. Ye, D. Z. Yang and S. Y. He, *Tribol. Lett.* 2010, **40**, 139.

35 T. Fujii, F. M. F. de Groot, G. A. Sawatzky, F. C. Voogt, T. Hibma and K. Okada, *Physical Review B* 1999, **59**, 3195.

36 J. Maiti, N. Kakati, S. H. Lee and Y. S. Yoon, *J. Fluor. Chem.* 2012, **135**, 362.

37 K. Q. Peng, Y. Wu, H. Fang, X. Y. Zhong, Y. Xu and J. Zhu, *Angew. Chem.-Int. Edit.* 2005, **44**, 2737.

38 W. L. Wilson, P. F. Szajowski and L. E. Brus, *Science* 1993, **262**, 1242.

39 B. S. Zou, J. P. Wang, C. Liu, J. Z. Zhang and M. A. El-Sayad, *Physical Review B* 2000, **62**, 16595.

40 J. Yuan and D. Haneman, *J. Appl. Phys.* 1999, **86**, 2358.

41 A. P. Li, G. F. Bai, K. M. Chen, Z. C. Ma, W. H. Zong, Y. X. Zhang and G. G. Qin, *Thin Solid Films* 1998, **325**, 137.

42 L. Skuja, *J. Non-Cryst. Solids* 1994, **179**, 51.

43 S. M. Prokes, *Appl. Phys. Lett.* 1993, **62**, 3244.

44 G. G. Qin, Y. M. Huang, J. Lin, L. Z. Zhang, B. Q. Zong and B. R. Zhang, *Solid State Commun.* 1995, **94**, 607.

45 G. Qin and G. G. Qin, *J. Appl. Phys.* 1997, **82**, 2572.

46 K. J. An, H. S. Kim, J. B. Yoo and G. Y. Yeom, *Thin Solid Films* 1999, **341**, 176.

47 G. Boulousis, V. Constantoudis, G. Kokkoris and E. Gogolides, *Nanotechnology* 2008, **19,** 255301.

48 D. Nilsson, S. Jensen and A. Menon, *J. Micromech. Microeng.* 2003, **13**, S57.

49 K. Nakayama and T. Kobayashi, *Wear* 1996, **198**, 52.

50 N. Chekurov, K. Grigoras, A. Peltonen, S. Franssila and I. Tittonen, *Nanotechnology* 2009, **20**, 65307.

51 L. Sainiemi, H. Keskinen, M. Aromaa, L. Luosujarvi, K. Grigoras, T. Kotiaho, J. M. Makela and S. Franssila, *Nanotechnology* 2007, **18**, 505303.
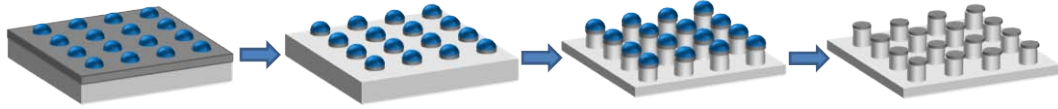
Scheme 1. Schematic diagram of the fabrication of Si nanopillar arrays: (A) hexagonal ordered iron oxide nanodots on Si substrate with a native oxide layer, (B) nanodots after SiO_2 etch, (C) nanopillars formed after Si etch and (D) Si nanopillars with a native oxide at top after removal of iron oxide.
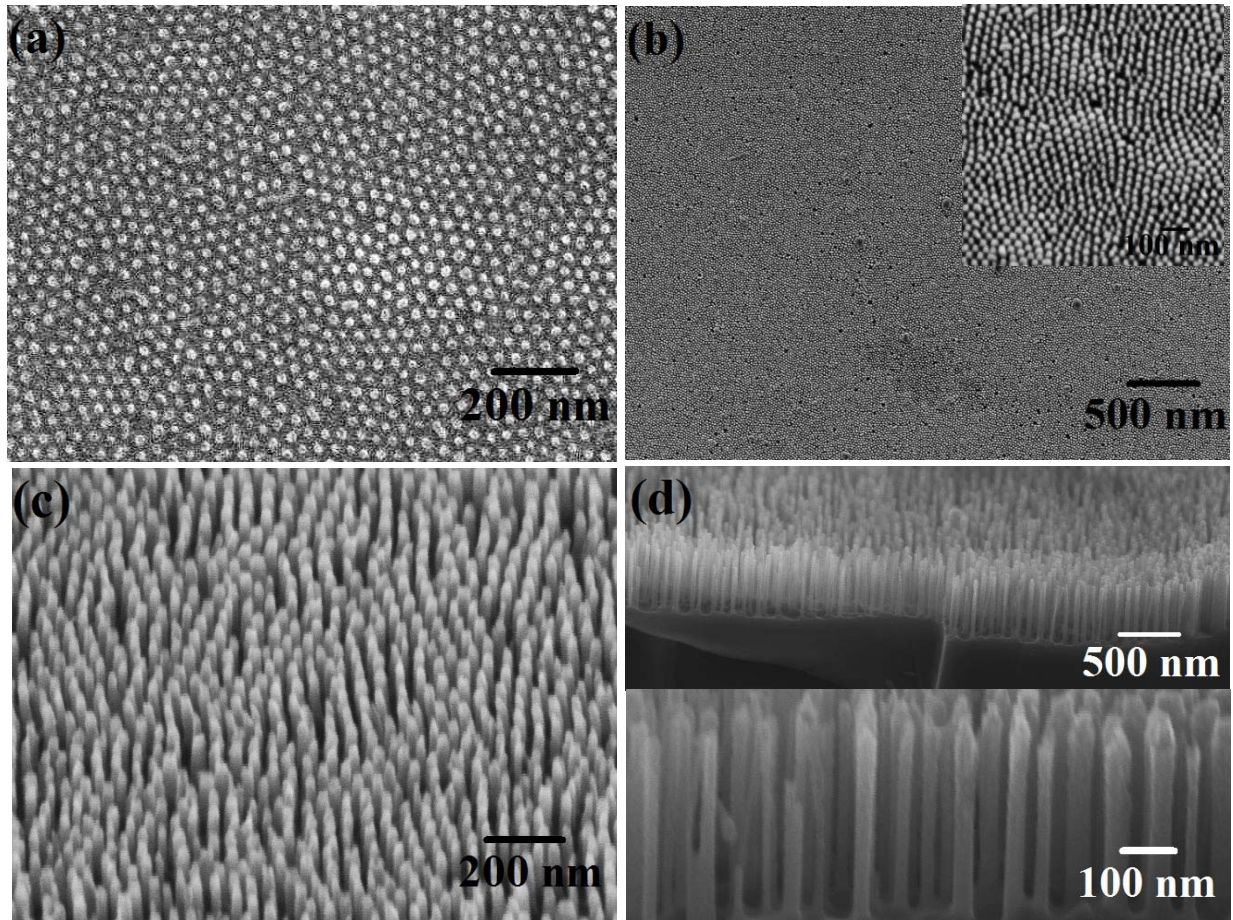
Fig. 1 SEM images of (a) hexagonal ordered iron oxide nanodots on Si substrate, (b) nanopillar arrays with iron oxide nanodots at top formed after pattern transfer onto silicon, (c) Si nanopillars after removal of mask and (d) cross-sectional image of 500 nm long Si nanopillars. Insets of (b) and (d) shows corresponding higher magnification SEM images revealing the hexagonal arrangement.
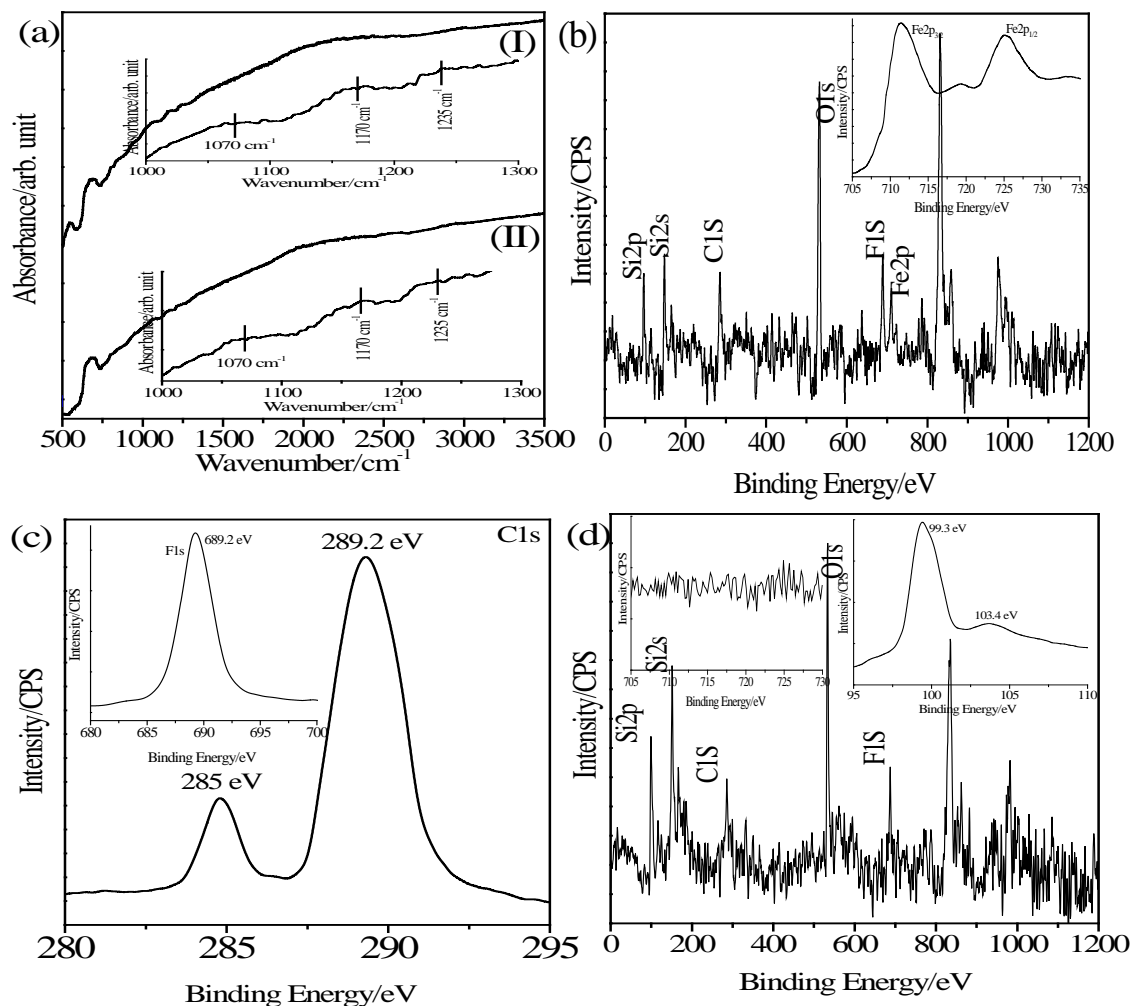
Fig. 2 (a) FTIR absorption spectra of the etched sample before (I) and after (II) iron oxide removal. Insets shows corresponding spectra in 100-1300 cm^{-1} range. XPS survey spectra of the nanopillars on Si substrate (b) before and (d) after removal of iron oxide. Insets of (b) and (d) shows corresponding high resolution Fe2p spectra. (c) and inset shows high resolution C1s and F1s spectra. Inset of (d)(right) illustrates Si 2p spectrum.
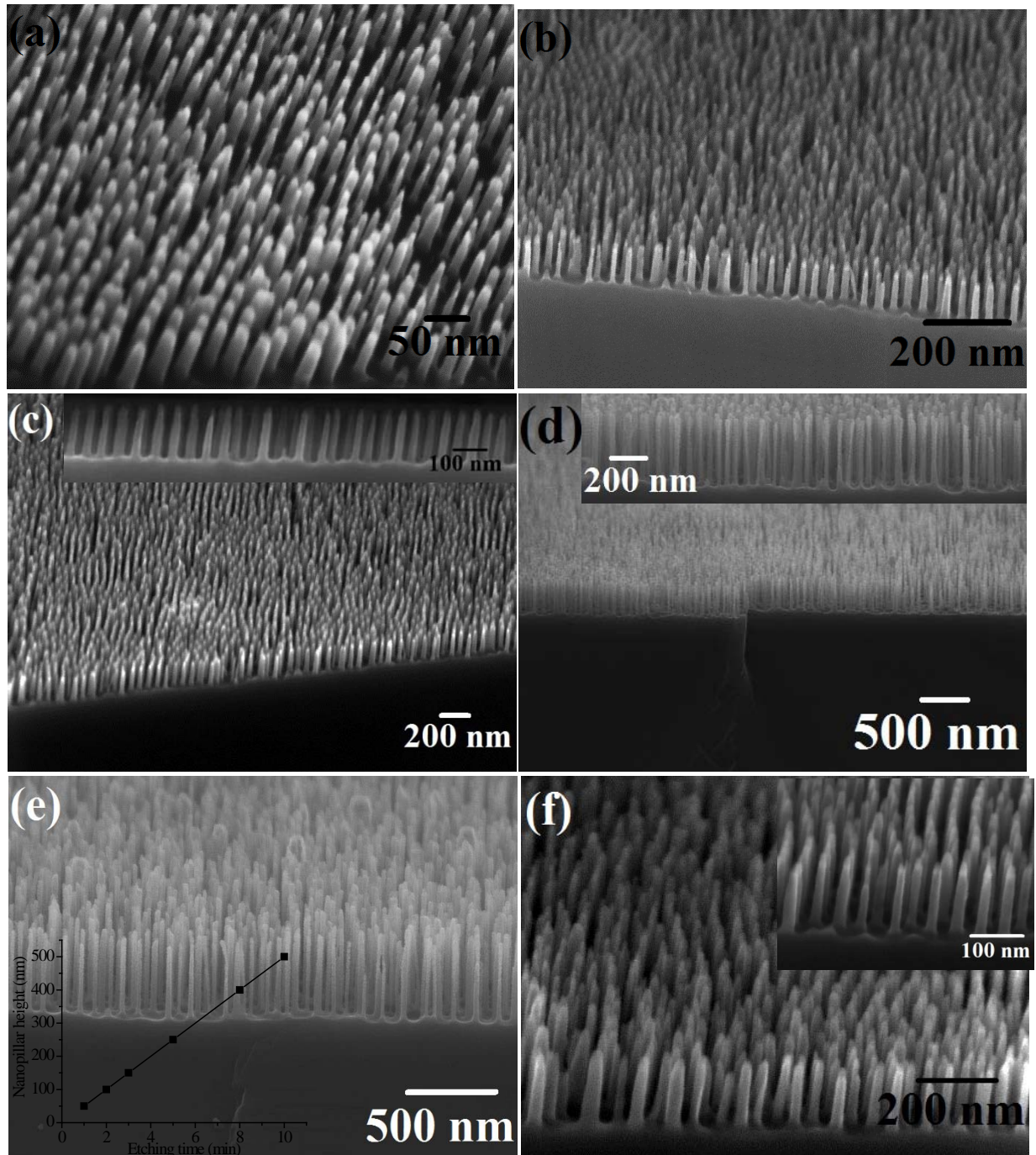
Fig. 3 Cross sectional SEM images of Si nanopillars with different diameter and height (a) 21 nm, 50 nm, (b) 21 nm, 100 nm, (c) 21 nm, 150 nm, (d) 21nm, 400 nm, (e) 21 nm, 500 nm, (f) 27 nm, 150 nm and (f, inset) 15 nm, 150 nm respectively. Inset of (c, d) shows oriented Si nanopillars with 42 nm spacing between them. Inset of (e) shows the variation of nanopillar height with etching time.
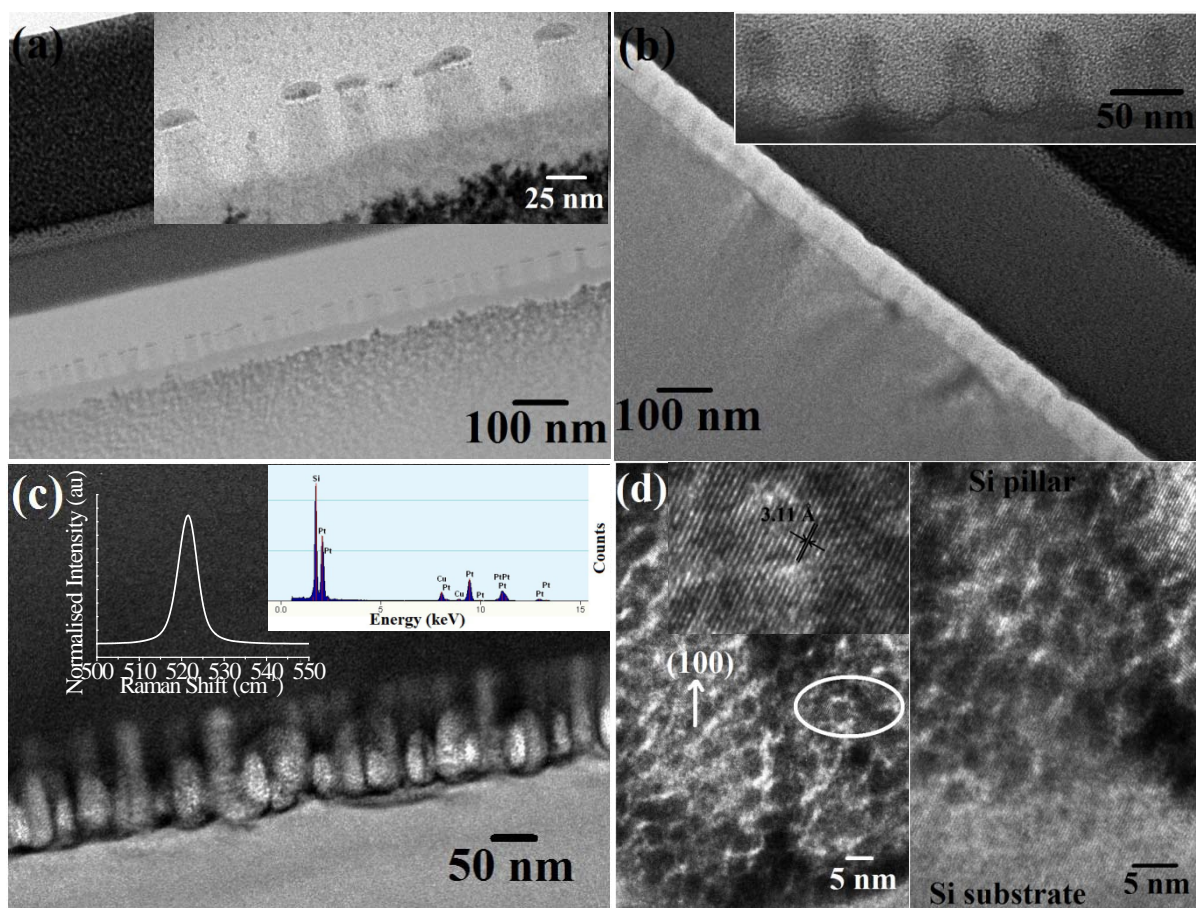
Fig. 4 Large area view of FIB thinned TEM cross sectional image of nanopillars on Si substrate (a) before and (b) after iron oxide removal process. Corresponding insets shows higher magnification TEM image, clearly depicts the presence and absence of iron oxide nanodots respectively. (c) TEM images of 150 nm long Si nanopillars arrays. Inset of (c)(right) EDAX spectrum along the length of a nanopillar. (d) HRTEM image shows continuous fringes across the junction of the nanopillar and Si substrate, Pt nanoparticles also noticeable deposited during preparation of FIB thinned sample. Inset of (c)(left) shows the Raman spectrum of Si nanopillar arrays on Si substrate.
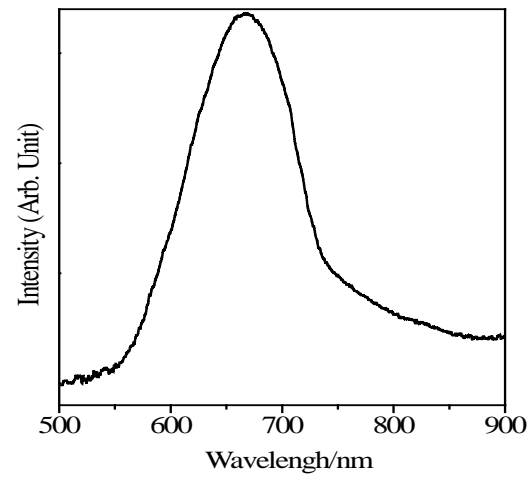
Fig. 5 PL spectrum of Si nanopillar arrays on Si substrate.

Graphical abstract:
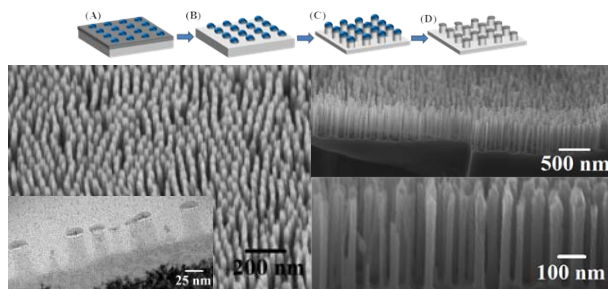
A novel, simple, cost effective and insitu hard mask technology is used to develop high aspect ratio silicon nanopillar and nanowire arrays over wafer scale. Iron oxide was found to be an excellent resistant mask over silicon. The nanopillars are crystalline with desirable uni-axial crystallographic orientation having uniform diameter and smooth sidewalls throughout their entire length. The aspect ratio of the nanopillars can be easily controlled.